Achieving ultrahigh crack resistance in glass through humid aging

Pengfei Liu,[1] Randall E. Youngman,[2] Lars R. Jensen,[3] Michal Bockowski,[4] and Morten M. Smedskjaer[1,*]

[1]*Department of Chemistry and Bioscience, Aalborg University, 9220 Aalborg, Denmark*
[2]*Science and Technology Division, Corning Incorporated, Corning, New York 14831, USA*
[3]*Department of Materials and Production, Aalborg University, 9220 Aalborg, Denmark*
[4]*Institute of High-Pressure Physics, Polish Academy of Sciences, 01–142 Warsaw, Poland*

(Received 26 February 2020; revised manuscript received 14 May 2020; accepted 22 May 2020; published 19 June 2020)

Oxide glasses continue to be among the most important materials for a sustainable society owing to their unique advantages, e.g., transparency, formability, low cost, and tailorable properties and functionalities. However, their high brittleness has severely been hindering the use of oxide glasses for many engineering and functional applications. Previous approaches to overcome this limitation by improving the fracture toughness have largely failed, but herein we report the use of a simple post-treatment, namely surface aging in a humid atmosphere, to improve not the resistance to crack growth, but rather the resistance to crack initiation. The effect of such aging on the mechanical performance is found to be highly composition dependent, and in stark contrast to most previous work, we thus find that water incorporation is not always a foe, but can also be a friend for glass mechanics. Specifically, we demonstrate crack-free ultrasharp cube corner indents in an aged caesium aluminoborate glass at loads above 25 N, while other aged oxide glasses studied in this work easily crack at loads below 1 N. The aging effect is found to be due to a combination of stress and hydrolysis assisted structural changes in the flexible aluminoborate glass network.

DOI: 10.1103/PhysRevMaterials.4.063606

I. INTRODUCTION

Oxide glasses continue to be among the most important engineering and functional manmade materials due to their useful properties, such as good transparency, relatively high hardness, and good chemical durability. Although the ultimate strength and ductility of defect-free amorphous oxides can be high [1,2], all known bulk oxide glasses are inherently brittle because of the lack of a stable shearing deformation mechanism and limited resistance to crack growth (low fracture toughness) [3–5]. To overcome this limitation, various postprocessing methods are used in industry, most notably thermal tempering [6] and chemical strengthening [7,8], with the aim to increase the critical stress needed for crack initiation and to retard the rate of crack growth by counteracting the stresses acting on the crack tip. In addition to adding extra cost, these methods are also limited to either relatively thick glasses (thermal tempering) or mobile ion-containing glasses (chemical strengthening). Alternatively, recent work has shown some promise in toughening oxide glasses by incorporating crystalline or glassy nanoparticles in the glass, but these treatments either require high pressure (and thus limits the sample size) or lead to a loss of transparency [9,10].

Another attractive strategy to overcome the limitations of brittleness is to enhance the damage or crack resistance through rational composition design [11–13]. Crack resistance (CR) here refers to the glass' ability to withstand stress without initiation of cracks upon sharp contact loading [14], specifically the load resulting in 50% probability of corner crack formation during indentation [14]. Such sharp contact deformation is a typical failure mode in the field for, e.g., cover glasses, and particularly radial cracks, propagating perpendicular to the glass surface, are believed to be important, as they can become the strength-limiting factor for many applications [15]. Recent examples of such tailored crack-resistant glasses include mixed modifier aluminosilicate [16], binary aluminosilicate [13], calcium boroaluminosilicate [17], tantalum aluminate [18], and alkali aluminoborate compositions [12,19]. On the other hand, post-treatment that increases the glass density (e.g., by low-temperature annealing or hot compression) typically leads to a decrease in CR [20]. Besides composition and post-treatment, it is known that other factors such as loading/unloading rate, surface quality, indenter tip geometry, time after unloading, and atmospheric conditions (temperature and humidity) also influence the crack resistance of glasses [21–23]. Particularly, the relative humidity (RH) plays a major role for the indentation response of glasses [23,24].

Understanding the details of glass-water interactions is thus crucial for tailoring the mechanical performance of oxide glasses. Besides water entry from a humid environment via diffusion or hydrolysis and condensation, water may already be present in the as-melted glass, e.g., as an impurity in the raw materials. Water typically exists in glasses in the form of either molecules or hydroxyl groups, depending on the glass composition and water content [25,26]. Wiederhorn [27] first studied the influence of atmospheric humidity on the cracking behavior of soda-lime-silicate glasses, and attributed the fatigue phenomenon to subcritical crack growth enhanced by

*Corresponding author: mos@bio.aau.dk

TABLE I. Overview of glass transition temperature (T_g), density (ρ), Young's (E) modulus, Poisson's ratio (υ), and Vickers hardness (H_v) for the present glasses prior to any aging.

Glass ID	Composition (mol %)	T_g (°C)	E (GPa)	υ	ρ (g/cm^3)	H_v (GPa)	Reference
CsAlB	$25Cs_2O$-$25Al_2O_3$-$50B_2O_3$	402	24.5	0.322	3.006	2.6	this work
NaAlB	$25Na_2O$-$20Al_2O_3$-$55B_2O_3$	451	46.5	0.291	2.240	3.3	[37]
LiAlBSi	$5SiO_2$-$25Li_2O$-$20Al_2O_3$-$50B_2O_3$	473	67.0	0.274	2.263	4.6	[38]
SLS	$13Na_2O$-$6MgO$-$10CaO$-$71SiO_2$	562	72.0	0.230	2.512	6.1	[39]
LaAlSi	$25La_2O_3$-$15Al_2O_3$-$60SiO_2$	862	113.7	0.305	4.336	7.2	[40]
LaAlB	$25La_2O_3$-$15Al_2O_3$-$60B_2O_3$	658	107.4	0.298	3.998	7.1	[40]

stress corrosion, in which the silicon-oxygen bond is assumed to undergo a hydrolysis reaction. Later work has shown that water entry during indentation leads to softening [28], molecular water surrounding the crack tip can lower the fracture toughness [29,30], and stress corrosion under high humidity increases the crack initiation probability [31]. On the other hand, water penetration has also been shown to inhibit crack growth in silica glass by shielding the crack tip due to network swelling [32,33] and result in fast stress relaxation [34].

Indeed, a few recent studies have shown that prehydration of a glass surface can increase the crack resistance for certain compositions. Namely, hydrothermal treatment (150 °C at 100% RH for 3 days) of soda-lime-silica (window) glass increases CR from around 0.5 to 3 N [35], while a lower temperature aging (22 °C at 85% RH for 30 days) increases CR from 50 to 100 N of some phosphoaluminosilicate glasses, but not for others [36]. Our recent study on a caesium aluminoborate glass shows an increase in CR from around 30 to >100 N upon low-RH treatment (23 °C at 45% RH for 7 days) [24], i.e., surface aging in a humid atmosphere. There is thus a strong composition dependence of the hydration-induced increase in CR and we infer that favorable intrinsic mechanical properties (prior to aging) likely need to be combined with a tailored propensity to undergo surface hydration to achieve the ultrahigh CR values. If the glass hydrates too rapidly, a white surface layer will form. For future applications, it would thus be beneficial if the surface could be prehydrated at high-RH conditions, but not undergo further pronounced hydration when taken back to ambient conditions.

In this work, we aim to understand these phenomena further by performing controlled low-temperature aging experiments of a metaluminous caesium aluminoborate glass. Compared to our recent work [24], we here perform much more detailed structural and mechanical characterization on samples with varying degree of aging. We also compare the aging behavior of the caesium aluminoborate glass with that of various oxide reference glasses (see Table I), which have been chosen to exhibit a wide range of network rigidity, as evidenced by the large span in glass transition temperature (from ∼400 to 860 °C) and hardness (from ∼2.6 to 7.2 GPa). Since aluminoborate glasses are known to be self-adaptive by easily changing the coordination numbers of Al and B under stress [12], we also perform aging experiments on a permanently densified caesium aluminoborate glass, which shows limited densification during subsequent indentation. We thus compare aging effects in both as-made and compressed glasses in order to decipher the role of coordination number changes on crack resistance. These changes are possible in the as-made glasses, but to a much smaller extent in the compressed glasses. Using a combination of mechanical characterization, solid-state nuclear magnetic resonance (NMR) spectroscopy of ^{11}B, ^{27}Al, and ^{133}Cs, and micro-Raman spectroscopy analyses of aged and densified glasses, we then show how a combination of stress and hydrolysis assisted structural changes in the flexible aluminoborate glass network is responsible for its ultrahigh crack resistance. These findings have important implications for utilizing humid aging as a simple post-treatment method to improve the fracture resistance of oxide glasses.

II. EXPERIMENT

A. Glass synthesis

We have prepared a bulk glass with nominal composition (in mol %) of $25Cs_2O$-$25Al_2O_3$-$50B_2O_3$ using the traditional melt-quenching technique. The composition is similar to that in our recent study [24], but here designed to have a lower fraction of tetrahedral boron (due to $[Cs_2O] = [Al_2O_3]$), which has been found to give a high CR value in sodium aluminoborate glasses [37]. The utilized raw materials were Al_2O_3 (99.5%, Sigma-Aldrich), H_3BO_3 (⩾99.5%, Honeywell International), and Cs_2CO_3 (99.5%, Sigma-Aldrich). First, the raw materials were weighed and thoroughly mixed. To prevent excessive foaming, the mixture was stepwise added to a Pt-Rh crucible and heated to around 800 °C in an electric furnace to remove the excess H_2O and CO_2. Subsequently, in order to homogenize the melt, the mixture was melted at 1070 °C for 2 h in air. Finally, it was poured onto a steel plate for quenching. The obtained glasses were immediately transferred to a preheated annealing furnace at 405 °C (estimated glass transition temperature) for 30 min, and then slowly cooled to room temperature. The composition of the glass was analyzed by inductively coupled plasma optical emission spectroscopy for Al_2O_3 and B_2O_3, and flame emission spectroscopy for the Cs_2O content, and found to be $24.5Cs_2O$-$24.1Al_2O_3$-$51.4B_2O_3$.

For comparison with the caesium aluminoborate glass (named CsAlB hereafter; see Table I), we also prepared five reference glasses based on our previous studies. All glasses' nominal chemical compositions and their measured properties are shown in Table I. These reference glasses include sodium aluminoborate glass ($25.5Na_2O$-$20.4Al_2O_3$-$54.1B_2O_3$) [37],

lithium silicoaluminoborate glass ($5SiO_2$-$25Li_2O$-$20Al_2O_3$-$50B_2O_3$) [38], a soda-lime-silica float glass ($13Na_2O$-$6MgO$-$10CaO$-$71SiO_2$) [39], lanthanum aluminosilicate glass ($25La_2O_3$-$15Al_2O_3$-$60SiO_2$) [40], and lanthanum aluminoborate glass ($25La_2O_3$-$15Al_2O_3$-$60B_2O_3$) [40]. These glasses were also produced by melt quenching, with the details given in the corresponding references [37,40].

Following determination of the glass transition temperature (T_g; see Sec. II C), all the glasses were reannealed for 30 min at their measured T_g and cooled down to room temperature at a cooling rate of approximately 3 K/min. After reannealing, samples were cut for the needed dimensions for density, modulus, x-ray diffraction, ultraviolet-visible (UV-VIS) spectroscopy, Raman spectroscopy, and indentation experiments (see Sec. II C). Subsequently these samples were optically polished in ethanol by using abrasive SiC disks (up to grit 4000). Finally, all the samples were kept in a desiccator to avoid hydration of the surface, or in a climate chamber to induce aging experiments (see Sec. II B).

B. Post-treatment: densification and aging

Following the treatment protocol described in previous work [41], the $24.5Cs_2O$-$24.1Al_2O_3$-$51.4B_2O_3$ glass samples were subjected to isostatic N_2-mediated pressure treatment at 1 GPa. The compression was carried out at its measured T_g (402 °C) for 0.5 h, and subsequent quenching with an initial cooling rate of 60 K/min. The pressure chamber was then decompressed at a 30-MPa/min rate. This gives rise to permanent volume densification, associated with both structural and property changes [41].

The present CsAlB glass (annealed and compressed version), as well as all the reference glasses were also subjected to controlled humid aging experiments in a climate chamber (WKL 100/40, Weiss) to hydrate their surfaces. Following our recent work [24], the aging experiment was done at 23 °C with 45% RH for varying duration up to 7 days. All the glass samples were immediately put into the climate chamber after being optically double-side polished in ethanol.

C. Basic property characterization

To confirm the amorphous nature, x-ray diffraction (XRD) patterns of the CsAlB glass were acquired (Empyrean XRD, PANalytical) from 0° to 70° at 40 kV with a scanning speed of 8°/min. The noncrystalline nature of the reference glasses has previously been confirmed [37,38,40]. Moreover, the chemical homogeneity of the CsAlB glass was investigated by acquiring micro-Raman spectra ranging from 250 to 1700 cm^{-1} (InVia, Renishaw) at five different surface locations that were separated by at least 1 mm. The measurements were done using a 532-nm laser with 10-s excitation time. The acquired spectra were subjected to baseline subtraction and normalization with respect to their area.

To confirm the incorporation of water in the CsAlB glass upon aging, we performed Fourier transform infrared (FTIR) spectroscopy measurements on a ground and polished sample with uniform thickness of 1.0 mm. The FTIR spectra were acquired using a Spectrum One spectrometer (PerkinElmer STA 6000) on a Ge crystal under ambient conditions with subsequent background subtraction. The absorption spectra (averaged over 64 scans) were collected in the wave-number region from 400 to 4000 cm^{-1}. The estimation of the water content in the oxide glasses is based on the Beer-Lambert law, which relates the concentration (by weight) of water in the glass (c_{H_2O}) to the absorbance of the FTIR beam through the glass (A), the samples thickness (Δx), and the molar absorption coefficient (ε_{H_2O}) related to the overall concentration of water in the glass [42]. The molar absorption coefficient of OH groups (ε_{OH}) is approximately equal to one-half of ε_{H_2O}. We do not know the actual values of ε_{OH} for the studied glasses, but previous studies [43] have shown that variations of ε_{OH} are of the same order of magnitude for various oxide glasses. Following the approach of Wu *et al.* [42], we calculate

$$c_{H_2O}\varepsilon_{OH} = \frac{AM_{H_2O}}{2\Delta x\rho}, \tag{1}$$

where M_{H_2O} is the molar mass of H_2O (18.02 g/mol) and ρ is the density of the glass (g/cm^3). That is, with this approach we are not relying on the absolute value of ε_{OH} to estimate variations in OH content among the samples.

T_g of the CsAlB glass was determined by differential scanning calorimetry measurements (STA 449 F3 Jupiter, Netzsch) at 10 K/min on specimens with a known thermal history (i.e., with a preceding cooling rate of 10 K/min). These samples were analyzed using Pt crucibles in argon (gas flow 60 mL/min). The intercept between the tangent to the inflection point of the endothermic peak and the extrapolated heat flow of the glass was interpreted as the onset of the glass transition (T_g). T_g values of the reference glasses were taken from the previous studies [37–40].

The density (ρ) of all glass samples was determined by Archimedes' principle of buoyancy. The weight of each specimen (at least 2 g) was measured in air and ethanol ten times. Based on the ratio between molar mass and density, we also calculated the molar volume (V_m). The elastic properties of the glasses were measured by ultrasonic echography using an ultrasonic thickness gauge (38DL Plus, Olympus) equipped with 20-MHz delay line transducers for the determination of the longitudinal V_1 and transversal wave velocities V_2. The detailed calculation method was shown in the previous study [38].

To evaluate whether the humid surface aging affects the visual appearance of the glass, we determined the optical transparency of the as-made and aged CsAlB glass on a 1.5-mm-thick sample. This sample was optically double-side polished in ethanol by using SiC disks (up to grit 4000) and then immediately transferred into the climate chamber for aging up to 7 days. Subsequently, the sample was analyzed in a UV-VIS spectrometer (Cary 50 Bio, Varian) every day, recording the transmission at wavelengths between 255 and 800 nm. We measured five different areas (at least 2 mm apart) of this sample to ensure the homogeneity. All UV-VIS transmittance spectra were normalized to 1 mm thickness.

D. Structural characterization

To study the structural changes induced by humid aging, we performed ^{11}B, ^{27}Al, and ^{133}Cs magic angle spinning

(MAS) NMR experiments for four different CsAlB glass samples: as-made/no aging, compressed/no aging, as-made/7 days aging, and compressed/7 days aging. Since the NMR measurements have to be done on powdered samples and the humid aging is expected to mostly affect the surface structure, the glasses were powdered with an agate mortar and pestle prior to aging (but not prior to hot compression, which is known to homogenously densify the bulk structure [44]). Aging of glasses for NMR spectroscopy was done by placing powdered glasses in a humidity controlled chamber (45% RH) at 23 °C for 7 days. After aging, the powdered glasses were sealed in glass vials to prevent further changes. ^{11}B, ^{27}Al, and ^{133}Cs MAS NMR experiments were conducted at 16.4 T using a commercial spectrometer (VNMRs, Agilent) and a 3.2-mm MAS NMR probe (Varian/Chemagnetics). The powdered samples were packed into 3.2-mm zirconia rotors, with sample spinning of 20 kHz for ^{11}B and 22 kHz for ^{27}Al and ^{133}Cs. ^{11}B and ^{27}Al MAS NMR data were collected at resonance frequencies of 224.5 and 182.3 MHz, respectively, utilizing radio-frequency pulses of 0.6 μs ($\pi/12$ tip angles), with 4-s recycle delay and signal averaging of 1000 acquisitions for ^{11}B MAS NMR, and a pulse delay of 2 s and collection of typically 600 scans for ^{27}Al MAS NMR. Additional ^{11}B and ^{27}Al MAS NMR data were acquired with ^{1}H decoupling to account for possible interactions in hydrated glasses, but these data were not different from the nondecoupled MAS NMR data, and therefore were not used further. ^{133}Cs MAS NMR data, at a resonance frequency of 91.8 MHz, were collected using short rf pulses (0.6 μs), recycle delays of 60 s, and accumulation of 400 scans for each experiment. MAS NMR spectra for ^{11}B and ^{27}Al were processed without any additional apodization, while those for ^{133}Cs benefitted from application of 100 Hz line broadening. MAS NMR data were plotted using the normal shielding convention and with shift referencing to aqueous boric acid (19.6 ppm) or aqueous aluminum nitrate (0 ppm). The latter shift referencing was also used for ^{133}Cs following the International Union of Pure and Applied Chemistry recommendation of using the ratio of frequencies for ^{27}Al and ^{133}Cs. ^{11}B MAS NMR data were fit with DMFit utilizing second-order quadrupolar line shapes for trigonal (B^{III}) resonances, and a combination of Gaussian and Lorentzian functions for the B^{IV} resonances. The overlapping satellite transition for the B^{IV} resonance was also fit and subtracted from the integration, yielding accurate site intensities for all B^{III} and B^{IV} peaks. The CzSimple model in DMFit was used to fit ^{27} Al MAS NMR data [45]. ^{133}Cs MAS NMR data were fit also with DMFit, using combinations of Gaussian and Lorentzian line shapes to reproduce the experimental data.

In addition to solid-state NMR spectroscopy analysis, we also acquired micro-Raman spectra of as-made and compressed CsAlB glasses with different aging condition, since this technique allows us to directly probe the medium-range structure as well as the structure of the surface regions deformed by indentation (see Sec. II E). Raman spectra were collected on an inVia micro-Raman spectrometer (Renishaw) with a 532-nm laser and an acquisition time of 10 s. The range of all spectra was from 250 to 4000 cm^{-1}, with resolution better than 2 cm^{-1}. The micro-Raman spectra were acquired around Vickers indents produced at 19.6 and 4.9 N, with increasing distances from the center to the edge of the Vickers indent. Two spectra were accumulated in each position to minimize the signal-to-noise ratio. All spectra were uniformly treated for background correction and area normalization.

E. Microindentation

We determined the Vickers hardness (H_V) and crack resistance (CR) of as-prepared, compressed, and aged glasses by using a CB500 microindenter (Nanovea). On each sample, ten Vickers indents with a load of 9.8 N (1 kgf) were generated to determined H_V. The loading duration and dwell time were set to 6 and 10 s, respectively. The residual imprints were subsequently analyzed with an optical microscope and H_V was calculated as

$$H_V = 1.8544 \frac{P}{\left(\frac{d_1+d_2}{2}\right)^2}, \tag{2}$$

where P is the contact load, and d_1 and d_2 are the lengths of the projected indent diagonals. We note that d_1 and d_2 were measured immediately after unloading (20–30 s), but as described in Sec. III B below, the indents of the CsAlB glass recover quickly. As such, the reported hardness of this glass may be higher than its "real value" due to humidity-induced recovery.

To evaluate CR, all glass samples were indented at different loads using both Vickers and cube corner diamond tip geometries. According to the method of Wada *et al.* [14], the probability of crack initiation (PCI) at each load was derived as the ratio between the number of corners with a corner crack and the total number of corners (4 for Vickers and 3 for cube corner). The crack resistance is defined as the load at which an average of 2 cracks for Vickers and 1.5 cracks for cube corner (PCI = 50%) occurred. On every specimen, at least ten indents were made by using the Vickers indenter tip (loading rate of 7.5 N/s and dwell time of 5 s) and cube-corner indenter tip (loading duration of 6 s and dwell time of 10 s). The measurements were conducted under laboratory conditions (room temperature, relative humidity of 50–55%).

In order to evaluate the effect of aging time on the indentation deformation mechanism of the CsAlB glasses and the other reference glasses, we determined the recovery of the indent side length over time. To do so, all samples were first optically polished in ethanol using SiC disks (up to grit 4000) and immediately afterwards indented ten times by a Vickers tip at a load of 4.9 N with loading duration of 6 s and dwell time of 10 s. Then images of the indents were recorded by means of the built-in microscope. After indentation and imaging, these samples were immediately transferred into the climate chamber (temperature: 23 °C, relative humidity: 45%) for aging, and then the existing indents were imaged once every day. The initial (20–30 s after unloading) indentation side length, $L_{s,i}$, was determined and then determined again after aging, $L_{s,a}$. Similarly to the recovery of indentation volume following the method of Yoshida *et al.* [46] to estimate densification contribution to overall indentation deformation [47], we calculate the aging-induced side length recovery (L_{AR}),

$$L_{AR} = \frac{L_{s,i} - L_{s,a}}{L_{s,i}}. \tag{3}$$

TABLE II. Effect of hot compression on density (ρ), molar volume (V_m), atomic packing density (C_g), elastic moduli [Young's (E), shear (G), and bulk (B) moduli], Poisson's ratio (υ), Vickers hardness (H_v), and Vickers crack resistance (CR) of the caesium aluminoborate glass without aging.

Glass	ρ (g/cm^3)	V_m (cm^3/mol)	C_g	E (GPa)	G (GPa)	B (GPa)	υ	H_v (GPa)	CR (N)
As prepared	3.006	43.58	0.511	24.5	9.3	22.9	0.322	2.6	58
Compressed	3.129	41.79	0.532	30.5	11.7	26.0	0.304	3.2	8
Error estimate	0.001	0.01	0.001	0.5	0.5	0.5	0.005	0.1	20%

III. RESULTS AND DISCUSSION

A. Glass formation and basic characterization prior to aging

Based on the x-ray-diffraction analysis (Fig. S1 in the Supplemental Material [48]), we find that there is no long-range-ordered structure in the as-prepared CsAlB glass. It also exhibits a typical glass transition in the heat capacity vs temperature curve with $T_g = 402\,^{\circ}$C (Fig. S2 in the Supplemental Material [48]). As seen from the micro-Raman spectra in Fig. S3 in the Supplemental Material [48], there are no significant differences among these across the sample surface, suggesting that the glass is compositionally homogeneous. Furthermore, the glass is found to be transparent in the wavelength range of visible light, with only minor changes in optical transmittance due to the surface aging at 45% RH (Fig. S4 in the Supplemental Material [48]). Table I shows the overview of T_g, density (ρ), Young's modulus (E), Poisson's ratio (υ), and Vickers hardness (H_v) for the as-prepared CsAlB glass and the other reference glasses. The CsAlB glass features a low glass transition temperature ($T_g = 402\,^{\circ}$C), low hardness ($H_v = 2.6$ GPa) and low Young's modulus ($E = 24.5$ GPa), but relatively high density ($\rho = 3.006$ g/cm^3) and high Poisson's ratio ($\upsilon = 0.322$) compared to the reference glasses. We note that the fracture toughness (K_{Ic}) of a compositionally similar caesium aluminoborate glass has recently been found to be 0.42 MPa m$^{0.5}$ [49].

To evaluate the water content in the as-melted CsAlB glass prior to aging, we consider the FTIR spectroscopy analysis (Fig. S5 in the Supplemental Material [48]). Almost all water in borate glasses is accommodated in the form of hydroxyl groups at relatively small concentrations of water [50], with the IR bands related to the stretching of B-OH groups present at wavelengths between 3600−3750 cm^{-1} and 3200−3500 cm^{-1} [50,12] depending on the glass composition. Based on Eq. (1), we calculate the value of $c_{H_2O}\varepsilon_{OH}$ in the CsAlB glass to be ∼0.49 (Fig. S6 in the Supplemental Material [48]) before aging, which is relatively low compared to that found in some soda lime borosilicate glasses [51]. As such, although the alkali aluminoborate glasses are known to feature low chemical durability compared to other oxide glasses [52], the water content of the as-made, polished glass is not unusually high and it may thus increase upon aging in humid atmosphere, i.e., the surface is not already fully hydrated prior to aging.

The effect of hot compression (prior to any aging) on ρ, molar volume (V_m), atomic packing density (C_g), E, shear modulus (G), bulk modulus (B), υ, H_v, and crack resistance (CR) of the CsAlB glass is summarized in Table II. To quantify changes in the free volume, we calculate the atomic packing density in addition to molar volume based on the ionic radii from Shannon [53] and the assumption of spherical atoms. C_g of as-prepared and densified CsAlB glasses is estimated to be 0.511 and 0.532, respectively, by assuming eightfold coordination for Cs, twofold coordination for O, and coordination numbers for B and Al based on the NMR results (see Table S1 in the Supplemental Material [48]). Upon volume densification (i.e., V_m decreases and C_g increases), the hardness of the glass increases, in agreement with previous work [44,54,55] on other oxide glasses. In addition to the structural changes upon densification (see Sec. III D), the denser structure gives rise to more atomic constraints per unit volume, which is known to increase hardness [44]. There is also a significant increase in all three elastic moduli upon hot compression, but a decrease in Poisson's ratio (Fig. S7 in the Supplemental Material [48]), as discussed in detail elsewhere for various oxide glasses [56].

B. Indent size recovery

Upon humid aging, we find that the water content of the CsAlB glass increases systematically with aging time (Fig. S6 in the Supplemental Material [48]), showing that atmospheric water permeates into the glass. It is also confirmed by the thermogravimetric analysis (Fig. S8 in the Supplemental Material [48]). This has important consequences for its mechanical behavior.

First, to understand the deformation mechanism of both the as-made and densified CsAlB glass relative to that of the other reference glasses, we consider the change in size of the Vickers indent as a function of aging time. Figure 1(a) shows representative optical images of 4.9-N indents on the surface of the as-made and densified CsAlB glass before and after aging for 7 days at 45% RH. The indents in both the as-made and densified glasses exhibit significant shrinkage upon aging, as also found in our recent study of an as-made peralkaline caesium aluminoborate glass [24]. In fact, even the images recorded immediately (20–30 s) after indentation unloading do not show the perfect square shape, indicating recovery already during the unloading process. However, the predensified CsAlB glass shows less indent size recovery upon aging, possibly because its dense structure allows for less water penetration to induce the indent volume recovery [44].

Figure S9 in the Supplemental Material [48] shows the time evolution of the indent size and shape of the as-made glass upon aging. With increasing aging time, the size of the indent becomes monotonically smaller, and the edge of the indent appears to have recovered above the original glass

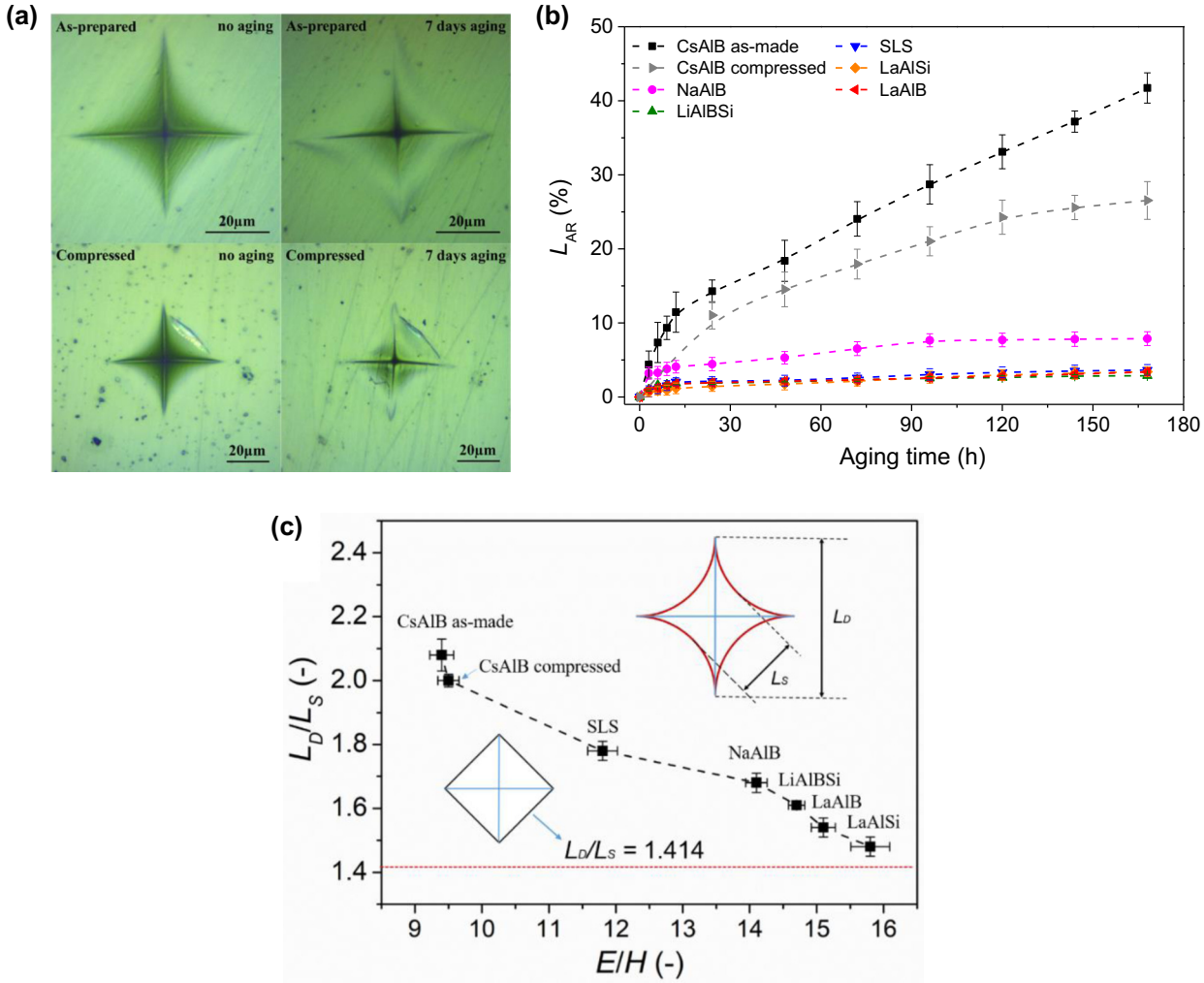

FIG. 1. (a) Optical images of Vickers indents produced at 4.9 N on the surface of the as-prepared glass and the compressed glass at 1 GPa before and after aging for 7 days. (b) Side length recovery (L_{AR}) of indents produced at 4.9 N as a function of aging time for all the investigated glasses. (c) Dependence of the bow-in parameter (L_D/L_S ratio) of Vickers indents produced at 4.9 N on the elastoplastic ratio (E/H) for all the investigated glasses before aging. The red dashed line represents the theoretical minimum L_D/L_S value (i.e., the case with no bow-in).

surface. As a consequence of the continuous recovery of the indent size and shape in a humid atmosphere, we cannot apply the traditional method by Yoshida *et al.* [46] for quantification of the densification contribution to the indentation volume based on annealing and volume recovery experiments. To quantify the rate of indentation recovery in the CsAlB glass and compare it with that of the reference glasses, we measure the aging time dependence of the recovery of the indentation side length (L_{AR}). The results are shown in Fig. 1(b). The qualitative observation of the indent self-recovery in the as-made and densified CsAlB glasses are confirmed by the aging time dependence of L_{AR}. We also note the limited indent size recovery in the other reference oxide glasses. Only the NaAlB glass shows recovery above 5%, pointing to the unusual indent recovery behavior of the CsAlB glass. For this composition, we note that a large fraction of the recovery occurs during the very early stages of the aging (i.e., first data point after unloading), but the shrinkage gradually continues even after 7 days of aging.

Next, we consider the interplay of the glasses' elastic vs aging-induced recovery of the indent shape by evaluating the bow-in parameter (L_D/L_S ratio), which exhibits systematic composition dependence. Figure 1(c) shows the dependence of L_D/L_S of indents produced at 4.9 N on the elastoplastic ratio (E/H) for all the investigated glasses before aging. By measuring the indent diagonal length (L_D) and the opposite side length (L_S), the elastic response of the material surrounding the indentation-induced cavity can be quantified by calculating the L_D/L_S ratio [57]. This bow-in parameter exhibits a negative linear scaling with the elastoplastic ratio E/H, in agreement with previous work [19]. The CsAlB glass has a very high bow-in parameter, close to that (2.2) of polydimethylsiloxane [57], which is likely due to a combination of elastic recovery and aging during unloading.

Finally, we study the aging time dependence of the Vickers hardness of the CsAlB glass (Figs. S10 and S11 in the Supplemental Material [48]). Vickers hardness first increases slightly with the aging time in the early stage of the aging, in which atmospheric water permeates into the glass at a high rate (Fig. S6 in the Supplemental Material [48]). This results in larger indent recovery during unloading, and thus smaller residual imprint and a higher apparent Vickers hardness. With

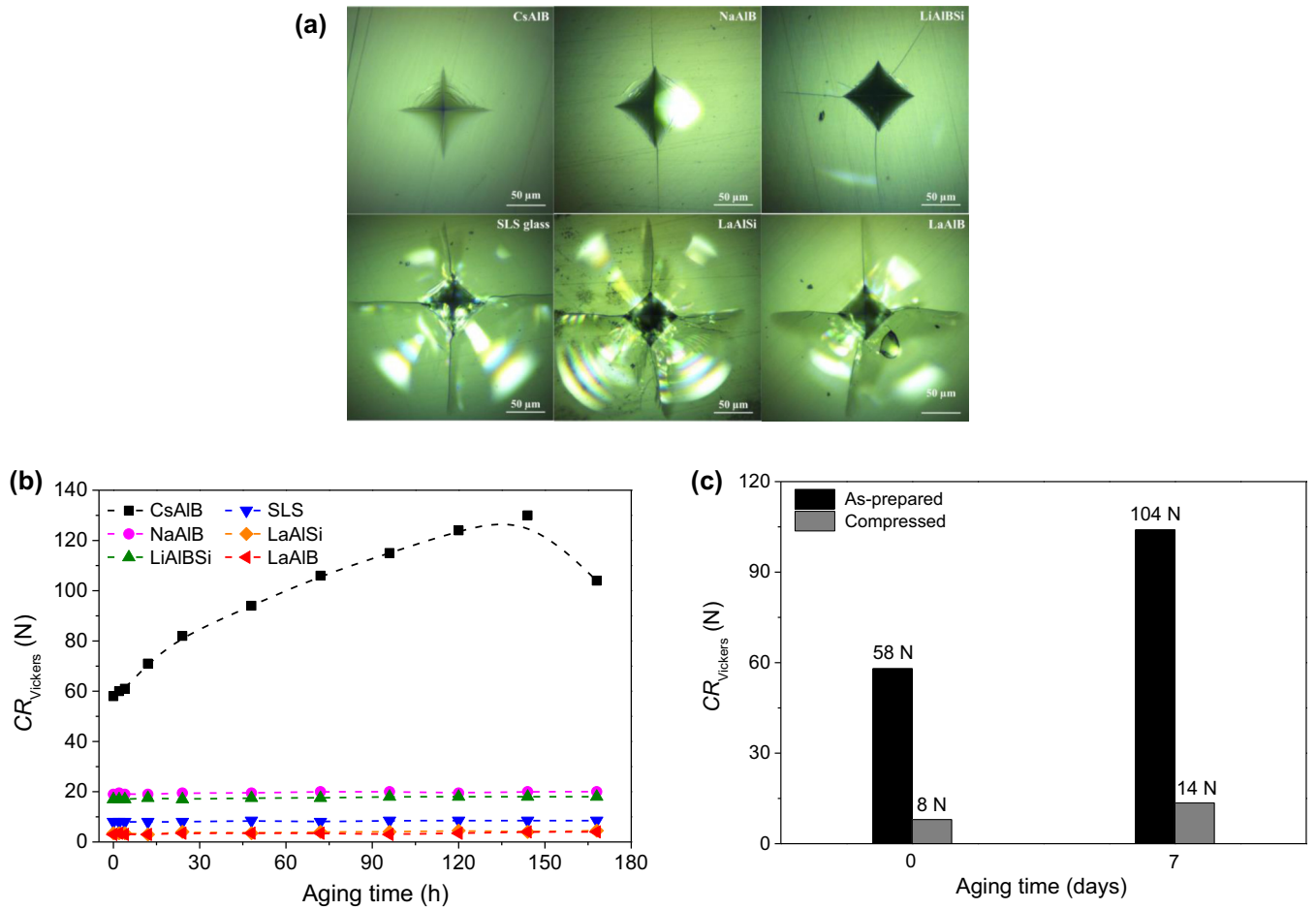

FIG. 2. (a) Optical images of Vickers indents produced at 19.6 N on the surface of all the investigated glasses prior to aging. (b) Crack resistance for Vickers indentation ($CR_{Vickers}$) as a function of aging time for all the investigated glasses. (c) $CR_{Vickers}$ of the as-prepared and compressed CsAlB glasses with aging for 0 or 7 days. The estimated error in crack resistance is around ±20%.

increased aging time, the rate of atmospheric water permeation decreases, resulting in the smaller relative recovery during unloading. The depolymerizing effect of water on the glass network likely causes the slight decrease in Vickers hardness for the longer aging time.

C. Indentation cracking resistance

In our previous studies [12,24,37], aluminoborate glasses have been found to generally feature high resistance to crack initiation. Especially the previously studied peralkaline caesium aluminoborate glass features high CR > 100 N, depending on the aging conditions [24]. Here, we systematically investigate the effect of surface hydration on the crack initiation behavior of various oxide glasses by studying the indentation behavior of both freshly polished (in ethanol) surfaces and those that have undergone aging at 45% RH for up to 7 days. Figure 2(a) shows optical images of Vickers indents produced at 19.6 N on the various oxide glasses prior to aging. We note that this applied load is insufficient to induce corner cracking in the as-made CsAlB glass, while corner cracks are visible in the other reference oxide glasses, highlighting the high CR of the CsAlB glass even before aging.

Figure 2(b) shows the effect of aging duration on the CR for Vickers indentation of all the as-made glasses, while examples of PCI vs load curves used to determine CR are given in Fig. S12 in the Supplemental Material [48]. We find that CR of the CsAlB glasses increases from around 58 N prior to aging to around 130 N after 6 days of aging. The preaging CR value is higher than that of the previously studied peralkaline caesium aluminoborate glass, while the 1-week aged CR value is smaller than that of the peralkaline caesium aluminoborate glass [24]. This could be because the peralkaline composition ($[Cs_2O] > [Al_2O_3]$) has more tetrahedral boron (∼8% B^{IV} of 55 mol % B_2O_3) [19] than the present metaluminous glass (∼5% B^{IV} of 51 mol % B_2O_3), giving rise to a more rigid and less self-adaptive network prior to aging [37]. For the other reference glasses, the surface aging at 45% RH has an almost negligible effect on the CR. For the as-made CsAlB glass, when the aging time reaches 6 days, CR reaches an apparent maximum value. During aging, the network should expand, driven by a structural relaxation towards lower potential energy state (from intact dense network to a looser hydrolyzed network), corresponding to relaxation of the indent cavities. We note that the indent cavities continue to recover and expand beyond 6 days (see Fig. S9 in the Supplemental Material [48]), indicating that the atmospheric water is continuously entering the glass surface [58]. As such, it is possible that the hydrated surface after long-term aging

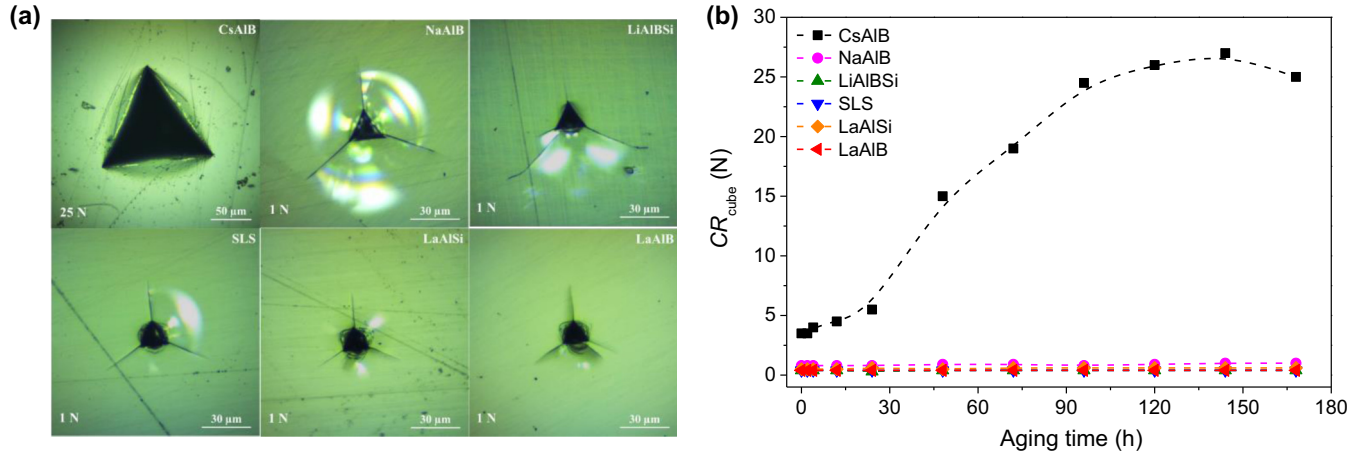

FIG. 3. (a) Optical images of cube corner indents produced at 25 N for as-made CsAlB and 1 N for the reference glasses after humid aging for 7 days. (b) Crack resistance for cube corner indentation (CR_{cube}) as a function of aging time for the as-made CsAlB and reference oxide glasses.

becomes sufficiently depolymerized to decrease CR due to the weaker network bonding.

Figure 2(c) shows the comparison of CR for the as-made and densified CsAlB glasses. Both before and after aging (7 days), the crack resistance is significantly lower in the densified glasses, which has previously been ascribed in other oxide glasses to the reduced ability of the densified glass to further densify during indentation [12]. In addition, the densified glass shows a smaller aging-induced increase in CR. Finally, we note that while the edge of the indent in the as-prepared glasses has recovered above the glass surface after aging [Fig. 1(a)], there is a smaller extent of indent size recovery in the compressed glass [Fig. 1(b)]. The reduced free volume in the compressed glass likely decreases the water intake, and thus limits the positive effect of humid aging on CR. This will be further investigated in Sec. III D.

Next, we consider the glasses' resistance to crack initiation under a sharper diamond tip, namely a cube corner indenter (three-sided pyramid with mutually perpendicular faces). This tip allows for less densification, higher residual stress, and easier crack initiation compared to the 136° four-sided pyramid Vickers diamond indenter [15]. Figure 3(a) shows the optical images of cube corner indents produced at 25 N for the as-made CsAlB glass and 1 N for the reference glasses after aging for 7 days. All the reference glasses already crack at all three corners at 1 N, while the CsAlB is able to survive indentation at more than ten times higher loading without cracking. The quantified cube corner crack resistance as a function of aging time is shown in Fig. 3(b), showing the same overall trend as that for Vickers crack resistance in Fig. 2(b). Namely, the CsAlB is highly affected by surface aging at 45% RH, while this is not the case for the selected reference glasses. All the glasses feature lower CR for cube corner than Vickers, with the aged CsAlB glasses having an ultrahigh crack resistance for cube corner (27 N) compared to that of the reference glasses (in the range of 0.4–1 N).

Finally, we consider the loading rate dependence of Vickers crack initiation probability for the freshly polished CsAlB glass and that aged for 7 days at 45% RH (Fig. 4). Normally, there is a higher crack initiation probability for longer indentation time [23]. Note that due to the large difference in CR before and after aging, the maximum load is not the same, but set to 30 and 90 N, respectively. We observe an anomalous increase in crack initiation probability with loading rate for the freshly polished CsAlB, but a normal decrease in crack initiation probability with loading rate for the aged sample. The highly stressed glass network is more vulnerable to the attack of water from the environment [24], and therefore, for the freshly polished glass, the relatively low loading rates allow sufficient time for the attack of water from the environment during the loading process. As discussed above, such water entry decreases the crack initiation probability for this glass (Figs. 2 and 3). On the other hand, the surface of the 7-days preaged glass has already been hydrated to a large extent, i.e., the extra time at lower loading rate does not lead to higher crack resistance. Instead the glass exhibits a normal loading rate dependence with less time for surface damage at higher loading rates.

D. Stress and Hydrolysis Induced Structural Changes in CsAlB

In order to understand the structural changes responsible for the ultrahigh crack resistance of the aged CsAlB glass and the significant effect of predensification on the aging behavior, we analyze the structure of densified and aged CsAlB samples using both micro-Raman and solid-state NMR spectroscopy. Figure 5 shows the micro-Raman spectra of the indented as-made and densified glasses with or without aging. These spectra were recorded at increasing distances (about 4 μm) from the center to the edge of a Vickers indent produced at 4.9 N. We divide the spectra into seven main band regions, with the expected assignments outlined in detail in Fig. S13 and Table S2 in the Supplemental Material [48].

Overall, we find that the surface becomes hydrated by exposure to ambient humid air, which manifests itself through the increase in intensity of the band region around 2850−3800 cm^{-1}, typically assigned to hydroxyl groups [59]. For the as-prepared glass, this band region increases

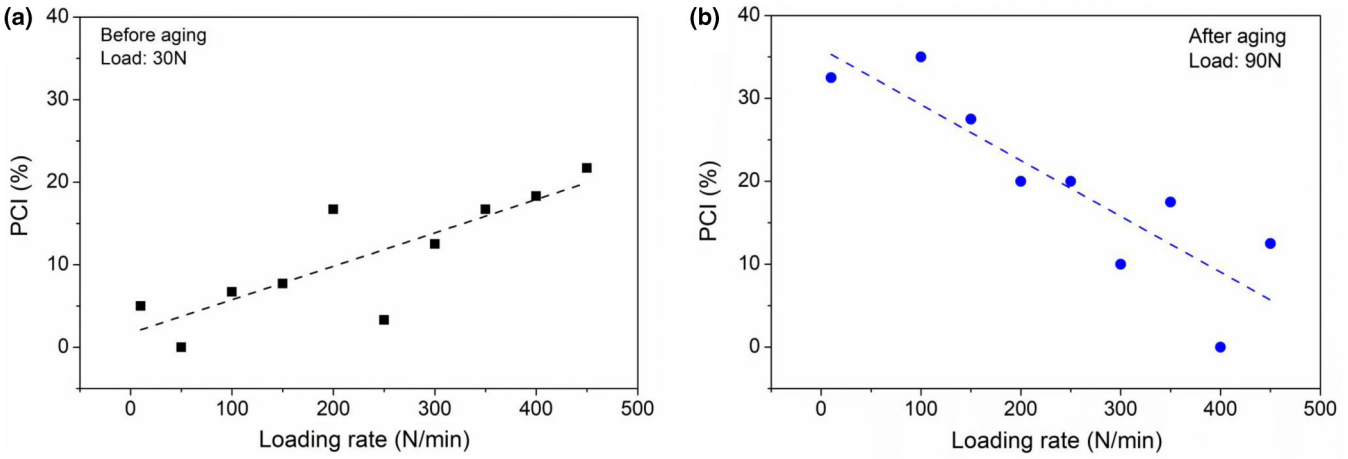

FIG. 4. Loading rate dependence of the Vickers crack initiation probability (PCI) for the CsAlB glass (a) before and (b) after aging for 7 days. The dashed lines are guides for the eyes.

observably in intensity after aging for 7 days, confirming the expectation that more atmospheric water permeates into the glasses with increasing aging time and thus supporting the indentation recovery behavior with aging time [Fig. 1(b)]. On the other hand, the region from ∼625 to 815 cm^{-1} is suppressed after aging, indicating that the borate superstructural units (diborates) are broken because of the hydrolyzation, i.e., the borate ring units are depolymerized into smaller ones. For the compressed glass with less free volume, the aging has a minor effect on the surface structure as detected by Raman spectroscopy (see Fig. S14 in Supplemental Material [48]), indicating less pronounced water permeation. This result may lead to the lower indentation side length recovery [Fig. 1(b)] and smaller CR [Fig. 2(c)] compared to the as-prepared CsAlB glass.

Considering next the indent position dependency of the structural changes in the glasses, we have calculated the relative area of the band region from ∼2850 to 3800 cm^{-1} at different positions. As shown in Fig. S15 in the Supplemental Material [48], the aging-induced increase in the hydroxyl-related band becomes less pronounced from position 1 to 5 [i.e., from high to low stress; see Fig. 5(a)], indicating that the material under the center of the indent is hydrated more quickly compared to the edge of the indent. This suggests that the highly stressed glass network is more vulnerable to the attack of water from the environment, in agreement

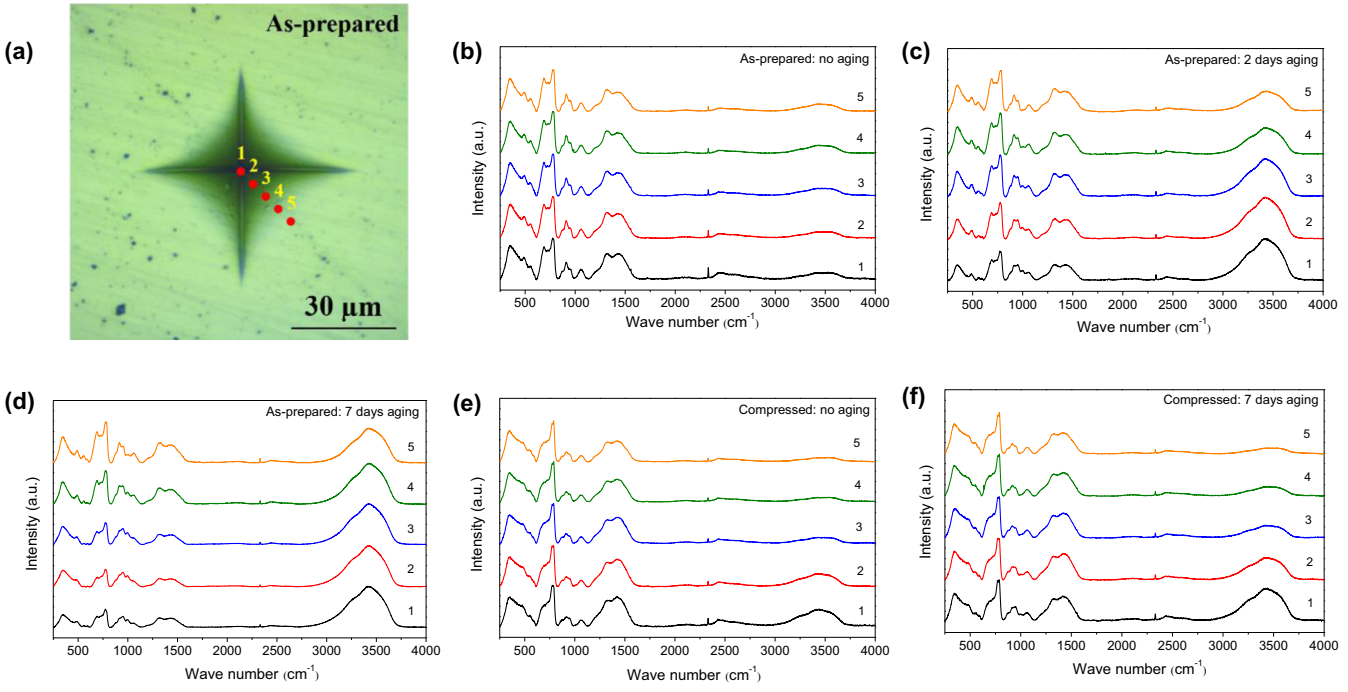

FIG. 5. Micro-Raman spectra of as-prepared CsAlB glass with aging for (b) 0, (c) 2, or (d) 7 days and compressed CsAlB glass with aging for (e) 0 or (f) 7 days. As shown in (a), the spectra were recorded at increasing distances (about 4 μm) from the center to the edge of a Vickers indent produced at 4.9 N.

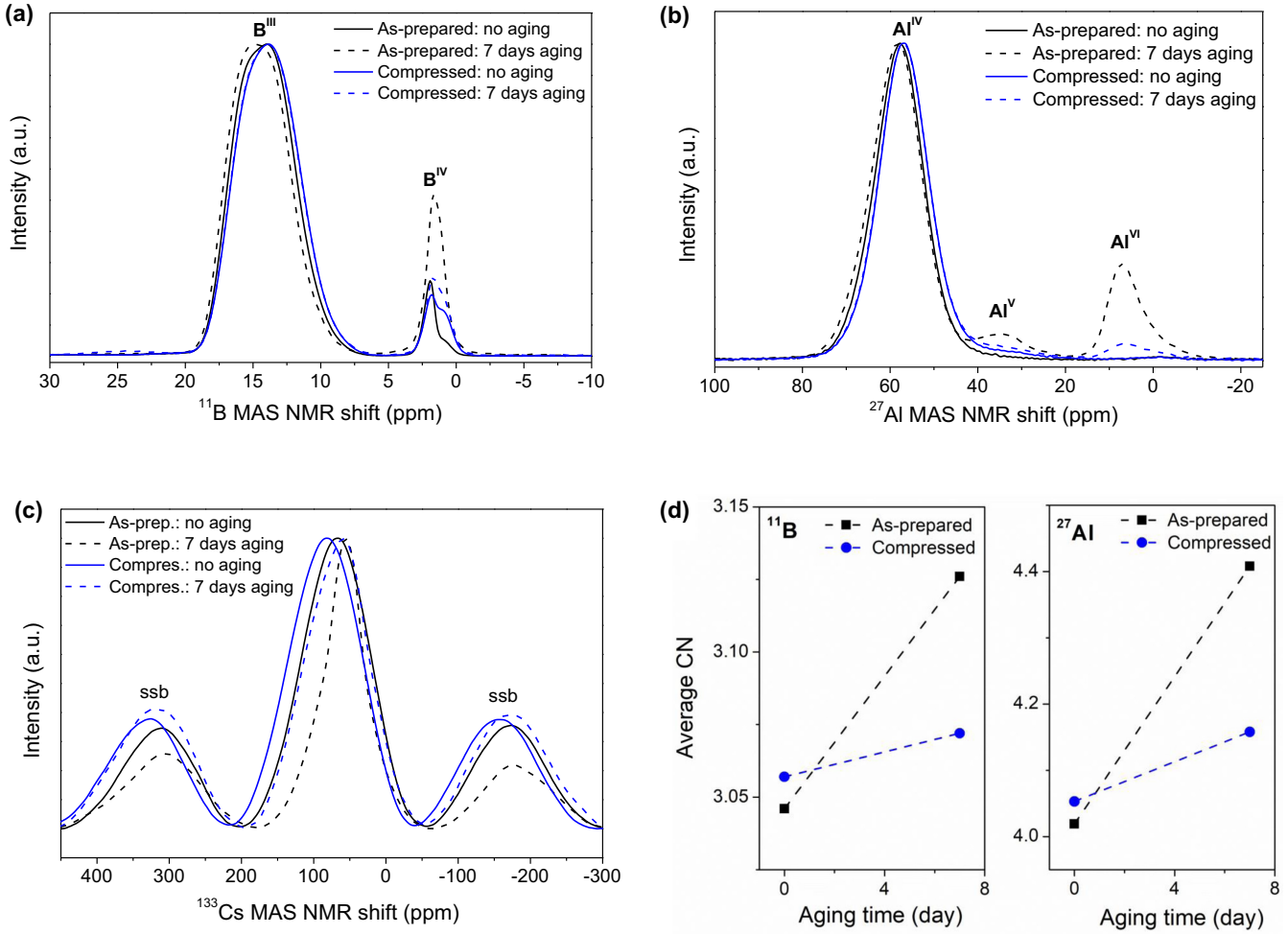

FIG. 6. (a) ^{11}B MAS NMR spectra for the as-prepared and compressed CsAlB glass with aging for 0 or 7 days. (b) ^{27}Al MAS NMR spectra for the as-prepared and compressed CsAlB glass with aging for 0 or 7 days. (c) ^{133}Cs MAS NMR spectra for the as-prepared and compressed CsAlB glass with aging for 0 or 7 days. Spinning sidebands (ssb) are indicated. (d) Effect of aging on the average coordination number (CN) of boron and aluminum in as-made and compressed glasses.

with previous studies on crack tips in oxide glasses, which are believed to propagate faster through the material once water can hydrolyze the strained network bonds [27,60]. Moreover, the extent of hydration increases with increasing indentation load, as seen by comparing the Raman spectra in Fig. 5(b) with those in Fig. S16 in the Supplemental Material [48]. This result supports that the highly stressed glass network is more vulnerable to the attack of water from the environment.

To further understand the effect of aging and pressure on the short-range structure of the studied CsAlB glasses, we performed ^{11}B, ^{27}Al, and ^{133}Cs MAS NMR spectroscopy measurements on powdered samples (Fig. 6). The determined speciation and spectral deconvolution are shown in Table S1 and Figs. S17 and S18, respectively, in the Supplemental Material [48]. Consistent with the preference for alkali modifier cations to charge-balance AlO_4^- relative to BO_4^- units in aluminoborate glasses [61–63], the network of the as-made glass consists mainly of B^{III} and Al^{IV}, with only minor fractions of higher coordinated boron and aluminum. Prior to any aging, this local chemical environment of the network-former atoms is sensitive to densification, as boron and aluminum can increase their coordination numbers with pressure [64,65]. Indeed, the ^{11}B and ^{27}Al MAS NMR spectra show that the average coordination numbers of B and Al increase upon compression [Fig. 6(d)], although the changes are much smaller than those observed in sodium and lithium aluminoborate glasses under the same pressure conditions [12]. Moreover, for the lithium aluminoborate glasses, the increase in coordination numbers of boron and aluminum is accompanied by a slight increase in ^{6}Li MAS NMR shift. In the present CsAlB glass, the ^{133}Cs MAS NMR shift also increases from 79 to 87 ppm upon 1 GPa hot compression [Fig. 6(c)]. This may be because the partial negative charge on the oxygen atom around boron increases with the pressure-induced conversion of B^{III} to B^{IV}, which is expected to increase their charge-compensation demand. Hence, the interactions between oxygen and caesium ions in the network become strengthened under the applied pressure, leading to a shrinkage of the average distance between oxygen and modifying cations. Moreover, since both aluminum and boron enter a higher coordination state with different need for charge compensation when the glass is compressed, some caesium cations are reassigned from charge-compensating Al^{IV} in the

as-made glass to charge-compensating B^{IV} in the compressed glass. Finally, we note that the majority of the trigonal boron signal in the as-made CsAlB glass can be assigned to ring sites (B^{III}_{ring}) [66,67], with the minor trigonal boron signal being assigned to nonring sites ($B^{III}_{nonring}$), as seen Table S1 in the Supplemental Material [48]. Support for the resolution and assignment of two types of B^{III} environments has been obtained from ^{11}B triple quantum MAS NMR analysis on the as-made glass (Fig. S19 in the Supplemental Material [48]), and the findings are consistent with numerous other studies of B-rich glasses. Upon compression, we find that the fraction of $B^{III}_{nonring}$ increases, accompanied by the conversion of B^{III} to B^{IV}, consistent with other borate and borosilicate glasses studied under similar densification treatments [12].

Next, we study the effect of aging on the structure of the as-made and densified CsAlB glasses. Generally the coordination numbers of Al and B increase upon aging, including the formation of sixfold Al [Figs. 6(a) and 6(b)], indicating that the local chemical environment of the network-former atoms is sensitive to hydrolysis. In the as-prepared glass, aging is found to have a more significant effect on the change of coordination numbers of Al and B compared to compression [Fig. 6(d)]. Assuming that the incorporated water acts as a traditional network modifier or charge compensator, it is unexpected that water simultaneously increases the fractions of B^{IV} (requires charge compensation) and Al^{V}/Al^{VI} (does not require charge compensation). As discussed above, alkali modifiers have an enthalpic preference for interaction with Al^{IV} over B^{IV} in aluminoborate glasses, but this is not observed upon aging if considering water as a modifier. Moreover, the ^{133}Cs MAS NMR spectra show water interaction with Cs modifiers and it is thus possible that water preferentially interacts with boron relative to aluminum (to form B^{IV}), while some of the Cs charge-compensators for Al^{IV} are removed by aging, effectively increasing the coordination number of aluminum. For the compressed glass, there is a minor change in the coordination numbers of Al and B upon aging compared to the as-prepared glass, in agreement with the Raman spectroscopy analysis, showing that less water molecules interact with the surface of the compressed glass upon aging. Finally, we note that the fraction of $B^{III}_{nonring}$ increases along with the conversion of B^{III} to B^{IV}, indicating that the water molecules hydrolyze the original ring structures of the borate network as the aging time increasing. This result is also in good agreement with the Raman spectroscopy analysis, showing that the borate superstructures are broken up upon aging.

Considering again the ^{133}Cs MAS NMR spectra in Fig. 6(c), we find that the main peak becomes sharper upon aging and shifts downwards (from 79 to 71 ppm), indicating that aging leads to an increase in the Cs-O bond distance. As seen in Fig. S20 and Table S3 in the Supplemental Material [48], the ^{133}Cs MAS NMR signal in the as-prepared and compressed glasses after aging can be deconvoluted into at least two distinct Cs^+ environments (sites I and II). Site I is the same as that in the as-made glass before aging, while the new site II is expected to be associated with hydrated Cs^+ groups attached to the glass network resulting from aging [68]. The latter interpretation is supported by several studies related to the impact of hydration on the ^{133}Cs NMR line shape [69,70], the effect of dehydration in titanosilicate minerals on the ^{133}Cs NMR spectra [71], the relation between Cs^+ mobility and motional narrowing of the ^{133}Cs resonance [72], and the role of hydration/dehydration on the ^{133}Cs quadrupolar coupling constant [73].

These Cs-OH groups could be more free to move around and thus have higher mobility in the surface of the glass, and would be consistent with both the relatively narrow and much more Lorentzian line shape for the Cs II site. In terms of the mechanical performance, such higher surface mobility is associated with higher network flexibility, as evidenced by the slightly lower hardness upon long-term aging (Fig. S10 in the Supplemental Material [48]). This effect is likely a contributing factor to the superior crack resistance of the aged CsAlB glass, as it could enable the indented glass to release the residual stress by structural rearrangements.

IV. CONCLUSIONS

We have shown that ultrahigh resistance to sharp contact cracking can be achieved in a caesium aluminoborate glass by simply storing the glass under typical atmospheric humidity (RH $\sim$ 45%) conditions. The same pronounced effect of humid aging on crack resistance is not found for a range of other tested oxide glasses. As the most significant finding, we have observed crack-free cube corner indents above 25 N in the aged caesium aluminoborate glass, which is the highest ever recorded crack resistance for cube corner indentation to our knowledge, even including commercial ion exchanged cover glasses. The caesium aluminoborate glass is characterized by a highly flexible network structure and upon subjecting the glass to permanent volume densification, the positive effect of humid aging on crack resistance almost vanishes. Our results indicate that the high crack resistance is due to the formation of surface hydroxyl groups, increasing coordination numbers of both Al and B, partial break down of the borate superstructures, and increasing average Cs-O bond distance upon aging. To realize the potential of using such glasses as damage-resistant engineering materials, the plasticity mechanism needs to be transferred to other oxide glass compositions that are suitable for large-scale manufacturing. The hydration layer would need to be formed by a post-treatment process at high relative humidity and/or temperature in order to ensure that the glass does not gradually corrode over time under ambient conditions.

ACKNOWLEDGMENTS

This work was supported by the China Scholarship Council (CSC No. 201806370210). We thank K. Januchta for providing some of the glass samples, and M. S. Bødker and C. Gao for assistance with the FTIR measurements.

[1] G. Brambilla and D. N. Payne, Nano Lett. **9**, 831 (2009).

[2] E. J. Frankberg, J. Kalikka, F. García Ferré, L. Joly-Pottuz, T. Salminen, J. Hintikka, M. Hokka, S. Koneti, T. Douillard, B. Le Saint, P. Kreiml, M. J. Cordill, T. Epicier, D. Stauffer, M. Vanazzi, L. Roiban, J. Akola, F. Di Fonzo, E. Levänen, and K. Masenelli-Varlot, Science **366**, 864 (2019).

[3] L. Wondraczek, J. C. Mauro, J. Eckert, U. Kühn, J. Horbach, J. Deubener, and T. Rouxel, Adv. Mater. **23**, 4578 (2011).

[4] J. E. Ritter and C. L. Sherburne, J. Am. Ceram. Soc. **54**, 601 (1971).

[5] C. R. Kurkjian, P. K. Gupta, and R. K. Brow, Int. J. Appl. Glas. Sci. **1**, 27 (2010).

[6] R. Gardon, Thermal tempering of glass, in *Elasticity and Strength of Glass, Glass: Science and Technology*, edited by D. R. Uhlmann and N. J. Kreidl, Vol. 5 (Academic Press, New York, 1980), pp. 146–217.

[7] V. M. Sglavo, A. Prezzi, and T. Zandonella, Adv. Eng. Mater. **6**, 344 (2004).

[8] S. Karlsson, B. Jonson, and C. Stålhandske, Glass Technol. **51**, 41 (2010).

[9] Q.-G. Jiang, C. Cao, T.-C. Lin, S. Wu, and X. Li, Adv. Mater. **31**, 1901803 (2019).

[10] Y. Zhang, L. Huang, and Y. Shi, Nano Lett. **19**, 5222 (2019).

[11] C. Moysan, R. Riedel, R. Harshe, T. Rouxel, and F. Augereau, J. Eur. Ceram. Soc. **27**, 397 (2007).

[12] K. Januchta, R. E. Youngman, A. Goel, M. Bauchy, S. L. Logunov, S. J. Rzoska, M. Bockowski, L. R. Jensen, and M. M. Smedskjaer, Chem. Mater. **29**, 5865 (2017).

[13] G. A. Rosales-Sosa, A. Masuno, Y. Higo, and H. Inoue, Sci. Rep. **6**, 23620 (2016).

[14] M. Wada, H. Furukawa, and K. Fujita, Crack resistance of glass on Vickers indentation, in *Proceedings of the 10th International Congress on Glass*, Vol. 11 (Ceramic Society of Japan, Tokyo, 1974), p. 39.

[15] S. Yoshida, J. Non-Cryst. Solids X **1**, 100009 (2019).

[16] J. Sehgal and S. Ito, J. Am. Ceram. Soc. **81**, 2485 (1998).

[17] T. M. Gross, J. Wu, D. E. Baker, J. J. Price, and R. Yongsunthon, J. Non-Cryst. Solids **494**, 13 (2018).

[18] G. A. Rosales-Sosa, A. Masuno, Y. Higo, H. Inoue, Y. Yanaba, T. Mizoguchi, T. Umada, K. Okamura, K. Kato, and Y. Watanabe, Sci. Rep. **5**, 15233 (2015).

[19] K. Januchta, M. Bauchy, R. E. Youngman, S. J. Rzoska, M. Bockowski, and M. M. Smedskjaer, Phys. Rev. Mater. **1**, 063603 (2017).

[20] K. Januchta and M. M. Smedskjaer, J. Non-Cryst. Solids X **1**, 100007 (2019).

[21] T. M. Gross and J. J. Price, Front. Mater. **4**, 4 (2017).

[22] S. Yoshida, K. Wada, T. Fujimura, A. Yamada, M. Kato, J. Matsuoka, and N. Soga, Front. Mater. **3**, 54 (2016).

[23] T. K. Bechgaard, J. C. Mauro, and M. M. Smedskjaer, J. Non-Cryst. Solids **491**, 64 (2018).

[24] K. Januchta, M. Stepniewska, L. R. Jensen, Y. Zhang, M. A. J. Somers, M. Bauchy, Y. Yue, and M. M. Smedskjaer, Adv. Sci. **6**, 1901281 (2019).

[25] J. Acocella, M. Tomozawa, and E. B. Watson, J. Non-Cryst. Solids **65**, 355 (1984).

[26] J. Luo, S. ichi Amma, L. Chen, D. Ngo, J. C. Mauro, C. G. Pantano, and S. H. Kim, J. Non-Cryst. Solids **510**, 179 (2019).

[27] S. M. Wiederhorn, J. Am. Ceram. Soc. **50**, 407 (1967).

[28] K. Hirao and M. Tomozawa, J. Am. Ceram. Soc. **70**, 497 (1987).

[29] J. M. Rimsza, R. E. Jones, and L. J. Criscenti, J. Geophys. Res. Solid Earth **123**, 9341 (2018).

[30] H. Mei, Y. Yang, A. C. T. van Duin, S. B. Sinnott, J. C. Mauro, L. Liu, and Z. Fu, Acta Mater. **178**, 36 (2019).

[31] S. Striepe, J. Deubener, M. M. Smedskjaer, and M. Potuzak, J. Non-Cryst. Solids **379**, 161 (2013).

[32] S. M. Wiederhorn, T. Fett, G. Rizzi, M. J. Hoffmann, and J. P. Guin, Metall. Mater. Trans. A: Phys. Metall. Mater. Sci. **44**, 1164 (2013).

[33] S. M. Wiederhorn, T. Fett, G. Rizzi, M. J. Hoffmann, and J. P. Guin, Eng. Fract. Mech. **100**, 3 (2013).

[34] M. Tomozawa and E. M. Aaldenberg, Phys. Chem. Glasses: Eur. J. Glass Sci. Technol., Part B **58**, 156 (2017).

[35] J. Luo, H. Huynh, C. G. Pantano, and S. H. Kim, J. Non-Cryst. Solids **452**, 93 (2016).

[36] T. M. Gross and G. M. Guryanov, US Patent No. 015,283,8A1 (2019).

[37] K. Januchta, R. E. Youngman, A. Goel, M. Bauchy, S. J. Rzoska, M. Bockowski, and M. M. Smedskjaer, J. Non-Cryst. Solids **460**, 54 (2017).

[38] P. Liu, K. Januchta, L. R. Jensen, M. Bauchy, and M. M. Smedskjaer, J. Am. Ceram. Soc. **103**, 944 (2020).

[39] T. Rouxel, J. Am. Ceram. Soc. **90**, 3019 (2007).

[40] K. Januchta, R. Sun, L. Huang, M. Bockowski, S. J. Rzoska, L. R. Jensen, and M. M. Smedskjaer, J. Non-Cryst. Solids **494**, 86 (2018).

[41] M. M. Smedskjaer, S. J. Rzoska, M. Bockowski, and J. C. Mauro, J. Chem. Phys. **140**, 054511 (2014).

[42] X. Wu and R. Dieckmann, J. Non-Cryst. Solids **357**, 2846 (2011).

[43] C. Peuker, W. Bessau, K. W. Brzezinka, A. Kohl, U. Reinholz, and H. Geibler, Glass Sci. Technol. **75**, 313 (2002).

[44] S. Kapoor, L. Wondraczek, and M. M. Smedskjaer, Front. Mater. **4**, 1 (2017).

[45] D. Massiot, F. Fayon, M. Capron, I. King, S. Le Calvé, B. Alonso, J.-O. Durand, B. Bujoli, Z. Gan, and G. Hoatson, Magn. Reson. Chem. **40**, 70 (2002).

[46] S. Yoshida, J.-C. Sanglebœuf, and T. Rouxel, J. Mater. Res. **20**, 3404 (2005).

[47] K. Januchta, P. Liu, S. R. Hansen, T. To, and M. M. Smedskjaer, J. Am. Ceram. Soc. **103**, 1656 (2020).

[48] See Supplemental Material at http://link.aps.org/supplemental/10.1103/PhysRevMaterials.4.063606 for further details about thermal, structural, and elastic properties of the studied glasses, including XRD spectra, DSC curves, UV-VIS transmittance spectra, FTIR spectra, micro-Raman spectra, ^{11}B triple quantum (3Q) MAS NMR data and deconvolution of the ^{133}Cs, ^{27}Al, ^{11}B MAS NMR spectra, aging time dependence of hardness and water content, and optical micrographs of Vickers indents. Also, it includes the following supplemental references: [S1] H. Li, Y. Su, L. Li, and D. M. Strachan, J. Non-Cryst. Solids **292**, 167 (2001); [S2] W. L. Konijnendijk and J. M. Stevels, *ibid.* **20**, 193 (1976); [S3] E. I. Kamitsos and G. D. Chryssikos, J. Mol. Struct. **247**, 1 (1991); [S4] B. N. Meera and J. Ramakrishna, J. Non-Cryst. Solids **159**, 1 (1993); [S5] K. Vignarooban, P. Boolchand, M. Micoulaut, M. Malki, and W. J. Bresser, Europhys. Lett. **108**, 56001 (2014); [S6] J. Krogh-Moe, J. Non-Cryst. Solids **1**, 269 (1969); [S7] P. McMillan and B. Piriou, *ibid.* **55**, 221 (1983); [S8] M. Licheron, V. Montouillout, F. Millot, and D. R. Neuville, *ibid.* **357**, 2796 (2011); [S9] T. Yano, N. Kunimine, S. Shibata, and M. Yamane, *ibid.* **321**, 137 (2003); [S10] R. K. Brow, D. R. Tallant, and G. L. Turner, J. Am. Ceram. Soc. **80**, 1239 (2005); [S11] A. Anedda, C. M. Carbonaro, F. Clemente, R. Corpino, P. C. Ricci, D. Fisica, V. Uni, and U. Cagliari,

J. Phys. Chem. B **107**, 13661 (2003); [S12] M. Mercier, A. Di Muro, D. Giordano, N. Métrich, P. Lesne, M. Pichavant, B. Scaillet, R. Clocchiatti, and G. Montagnac, Geochim. Cosmochim. Acta **73**, 197 (2009); [S13] N. Ollier, T. Charpentier, B. Boizot, G. Wallez, and D. Ghaleb, J. Non-Cryst. Solids **341**, 26 (2004); [S14] K. Januchta, M. Stepniewska, L. R. Jensen, Y. Zhang, M. A. J. Somers, M. Bauchy, Y. Yue, and M. M. Smedskjaer, Adv. Sci. **6**, 1901281 (2019).

[49] T. To, L. R. Jensen, and M. M. Smedskjaer, J. Non-Cryst. Solids **534**, 119946 (2020).

[50] C. Gautam, A. K. Yadav, and A. K. Singh, ISRN Ceram. **2012**, 428497 (2012).

[51] M. M. Smedskjaer, J. C. Mauro, and Y. Yue, J. Phys. Chem. B **119**, 7106 (2015).

[52] N. Mascaraque, K. Januchta, K. F. Frederiksen, R. E. Youngman, M. Bauchy, and M. M. Smedskjaer, J. Am. Ceram. Soc. **102**, 1157 (2019).

[53] R. D. Shannon, Acta Crystallogr. Sect. A **32**, 751 (1976).

[54] K. G. Aakermann, K. Januchta, J. A. L. Pedersen, M. N. Svenson, S. J. Rzoska, M. Bockowski, J. C. Mauro, M. Guerette, L. Huang, and M. M. Smedskjaer, J. Non-Cryst. Solids **426**, 175 (2015).

[55] M. N. Svenson, M. Guerette, L. Huang, N. Lönnroth, J. C. Mauro, S. J. Rzoska, M. Bockowski, and M. M. Smedskjaer, Chem. Phys. Lett. **651**, 88 (2016).

[56] M. B. Østergaard, S. R. Hansen, K. Januchta, T. To, S. J. Rzoska, M. Bockowski, M. Bauchy, and M. M. Smedskjaer, Materials (Basel) **12**, 2439 (2019).

[57] S. Yoshida, M. Kato, A. Yokota, S. Sasaki, A. Yamada, J. Matsuoka, N. Soga, and C. R. Kurkjian, J. Mater. Res. **30**, 2291 (2015).

[58] U. Bauer, H. Behrens, M. Fechtelkord, S. Reinsch, and J. Deubener, J. Non-Cryst. Solids **423-424**, 58 (2015).

[59] A. Anedda, C. M. Carbonaro, F. Clemente, R. Corpino, and P. C. Ricci, J. Phys. Chem. B **107**, 13661 (2003).

[60] T. Tomozawa, W. -T. Han, and W. A. Lanford, J. Am. Ceram. Soc. **74**, 2573 (1991).

[61] R. Gresch, W. Müller-Warmuth, and H. Dutz, J. Non-Cryst. Solids **21**, 31 (1976).

[62] L. Züchner, J. C. C. Chan, W. Müller-Warmuth, and H. Eckert, J. Phys. Chem. B **102**, 4495 (1998).

[63] L.-S. Du and J. F. Stebbins, Solid State Nucl. Magn. Reson. **27**, 37 (2005).

[64] M. N. Svenson, T. K. Bechgaard, S. D. Fuglsang, R. H. Pedersen, A. Ø. Tjell, M. B. Østergaard, R. E. Youngman, J. C. Mauro, S. J. Rzoska, M. Bockowski, and M. M. Smedskjaer, Phys. Rev. Appl. **2**, 024006 (2014).

[65] T. K. Bechgaard, A. Goel, R. E. Youngman, J. C. Mauro, S. J. Rzoska, M. Bockowski, L. R. Jensen, and M. M. Smedskjaer, J. Non-Cryst. Solids **441**, 49 (2016).

[66] R. E. Youngman and J. W. Zwanziger, J. Non-Cryst. Solids **168**, 293 (1994).

[67] R. E. Youngman and J. W. Zwanziger, J. Phys. Chem. **100**, 16720 (1996).

[68] B. R. Cherry, M. Nyman, and T. M. Alam, J. Solid State Chem. **177**, 2079 (2004).

[69] C. A. Weiss, R. J. Kirkpatrick, and S. P. Altaner, Geochim. Cosmochim. Acta **54**, 1655 (1990).

[70] X. Xu, A. G. Kalinichev, and R. James Kirkpatrick, Geochim. Cosmochim. Acta **70**, 4319 (2006).

[71] V. Luca, J. V. Hanna, M. E. Smith, M. James, D. R. G. Mitchell, and J. R. Bartlett, Microporous Mesoporous Mater. **55**, 1 (2002).

[72] H. Liu and C. P. Grey, Microporous Mesoporous Mater. **53**, 109 (2002).

[73] P.-J. Chu, B. C. Gerstein, J. Nunan, and K. Klier, ChemInform **18**, 3588 (1987).